Development of Low-noise Double-sided Silicon Strip Detector for Cosmic Soft Gamma-ray Compton Camera ⋆

Y. Fukazawa, T. Nakamoto, N. Sawamoto, S. Uno, T. Ohsugi [a] , H. Tajima, [b]
T. Takahashi, T. Mitani, T. Tanaka, and K. Nakazawa [c]

[a] *Department of Physical Sciences, Hiroshima University, 1-3-1 Kagamiyama, Higashi-Hiroshima, Hiroshima 739-8526, Japan*

[b] *Stanford Linear Accelerator Center, Menlo Park, CA, USA*

[c] *Institute of Space and Astronautical Science (ISAS), Aerospace Exploration Agency (JAXA), Sagamihara, Kanagawa 229-8510, Japan*

Abstract

Double-sided silicon strip detectors (DSSD) provide a very promising technology for constructing a Compton Camera, which is expected to provide a high-sensitivity soft gamma-ray observation in the 0.1–20 MeV energy range. The merits of DSSD are the high energy resolution, high scattering efficiency, low radio-activation in the orbit, moderate radiation hardness, smaller Doppler broadening, large size, and stable performance. A key feature for optimal performance is the low noise level of the DSSD and the attached frontend electronics. We minimized the noise by optimization of the electrode geometry of the DSSD. We have thus obtained an energy resolution of 1.3 keV (FWHM) for 60 keV and 122 keV at -10°C. It was found that the detection efficiency for gamma-rays was uniform over the DSSD and the signal charge split between neighboring strips was not significant. We also confirmed that the Compton imaging by two DSSDs achieved a good angular resolution close to the Doppler-broadening limit.

Key words: Silicon Strip Detector, Compton Camera, VA-chip, Gamma-ray detector
PACS: 07.85.-m, 07.85.Nc, 95.55.Ka

1 Introduction

Recent soft gamma-ray observations have revealed that the universe is rich in high energy phenomena, associated with supernova remnants, black holes, pulsars, clusters of galaxies, and gamma-ray bursts. Observations of nonthermal gamma-ray emissions is important to understand the physics of these phenomena. However, high-sensitivity observations in the energy range of 10 keV to 20 MeV have not been possible due to difficulties in detection, imaging, and background rejection. Recent developments of the hard X-ray telescope will improve the sensitivity below 80 keV, but the energy range between 0.1–20 MeV will still be unaffected. Since Compton scattering is the dominant photon-matter interaction, the Compton imaging telescope is the appropriate tool for studying this energy range. The COMPTEL on-board the Compton Gamma-Ray Observatory (CGRO) was the first instrument to use Compton imaging, and it was found to be very effective in the MeV gamma-ray observation. A more sophisticated technique for Compton imaging has become available, through the use of segmented semiconductor detectors, such as silicon strip detectors and CdTe (Cadmium Telluride) pixel detectors[1][2][3][4]. A multi-layer semiconductor detector allows good energy resolution, good angular resolution, compactness, small weight, high efficiency, and effective background rejection.

Compton imaging of gamma-rays is based on the measurement of detector records of scattered and absorbed photons. When the gamma-ray with an incident energy E_1 is scattered by the detector material, the scattering angle θ against the incident direction is constrained as

$$\cos\theta = 1 + \frac{m_e c^2}{E_1 + E_2} - \frac{m_e c^2}{E_2}$$

where E_2 and $m_e c^2$ are the energy of the scattered photon and the electron rest mass, respectively. The incident direction of one gamma-ray is constrained to a cone with the opening angle θ, and we can determine the source position by superposing the Compton cones of many events. The uncertainty of measurement of the recoil electron energy $E_1 - E_2$, that mainly determines the

⋆ The authors are grateful to K. Yamamura in Hamamatsu Photonics for fabrication of test silicon strip detectors. This work has been carried out under support of "Ground-based Research Announcement for Space Utilization" promoted by Japan Space Forum, U.S. Department of Energy, contract DE-AC03-76SF00515, and Grantin-Aid by Ministry of Education, Culture, Sports, Science and Technology of Japan (12554006, 13304014, 14079206, 14079207).

Email address: fukazawa@hirax6.hepl.hiroshima-u.ac.jp (Y. Fukazawa, T. Nakamoto, N. Sawamoto, S. Uno, T. Ohsugi).

angular resolution, is attributed to the detector energy resolution and to the Doppler broadening of the energy of the recoil electron caused by the orbital angular momentum of electrons bound to the atoms. The limit to the angular resolution induced by Doppler broadening is $\sim 4^\circ$ and $\sim 1^\circ$ for a gamma-ray energy of 100 keV and 500 keV, respectively, and the contribution of the detector energy resolution δE becomes important for $\delta E > 2$ keV (FWHM). We are developing a low-noise Compton camera with the energy resolution of $\sim$1.5 keV (FWHM) for the soft gamma-ray detector.

Our choice consists of a multi-layer semiconductor hybrid detector with double-sided silicon strip detectors (DSSD) and CdTe pixel detectors. The DSSD is suitable as a scattering material because it provides good position resolution, good energy resolution, high scattering efficiency and small Doppler broadening. Low radio-activation by protons in the orbit also helps us to achieve a low background level. At photon energies of 0.1–0.5 MeV, Compton scattering occurs mainly in the DSSD layers and the scattered photon is absorbed by the CdTe layers. In order to capture the scattered photon, the DSSD layers are surrounded by the CdTe detectors. At higher energy, multiple scattering frequently occurs, but tracking three hits of Compton scattering is sufficient to reconstruct the energy and the direction of the incident photon[1]. In order to achieve the required energy resolution, a low-noise multi-channel readout large-scale integration (LSI) is also a key feature. A detailed introduction and early demonstration have been reported by Tajima et al. (2002, 2003) and Mitani et al. (2003)[5] [6][7]. In this paper, we shortly describe the optimization of the detector components to improve the energy resolution, and demonstrate the good performance of Compton imaging. A detailed description of the performance of the DSSD and of the DSSD in combination with the CdTe pixels are reported in Fukazawa et al. (2004)[10] and Tanaka et al. (2004)[11], respectively.

2 Low noise DSSD system

The DSSD were designed with no bias resistors and AC coupling capacitances, to allow readout with DC coupled electronics. Alternatively, we used a dedicated chip (the RC chip) to provide biasing resistors and decoupling capacitances to the read-out electronics. The DSSDs and RC chips are fabricated by Hamamatsu Photonics, Japan.

We have produced nine types of silicon strip detector prototypes dedicated to this study, including single-sided p-strip detectors for R&D. In the double-sided strip detectors, n-strips are implanted orthogonal to p-strips on the other side, to provide two-dimensional information of the interaction position. The size and thickness of the detectors is 25.6×25.6 mm^2 and 300 μm, with a strip

pitch of 200–800 μm, and a strip gap of 100–160 μm. The input capacitance to the electronics is the main source of noise. In order to reduce the input capacitance to each readout channel, both p- and n-strips are split into two strips and read-out from both ends. The interstrip capacitance can be reduced by increasing the strip gap, at the price of a small increase of the leakage current. Different RC chips with bias resistors and AC capacitances between 1.0–6.0 GΩ and 22–110 pF, respectively, were produced and compared. The VA32TA is a 32-channel low-noise MOS amplifier that includes preamplifier, shaper, sample/hold, analog multiplexer, and discriminator. The VA32TA chip is processed by IDEAS ASA, Norway, and manufactured with 0.35 μm AMS technology to increase the radiation hardness[12]. The size of the frontend MOSFET of the preamplifier is optimized for low-noise operations. Majority selector circuits for the register to ensure tolerance against Single-Event Upset (SEU) is implemented for space applications. The electric power consumption is 6.3 mW/channel, and the pad pitch is 100 μm. A more detailed explanation of the VA32TA is given in Tajima et al. 2002[5].

We characterized each type of DSSD and RC chips by measuring the leakage current, depletion voltage, and total capacitance (interstrip plus bulk capacitance), in order to evaluate the noise performance[13]. The leakage current of all DSSDs is at most 0.1–0.5 nA per channel at room temperature, indicating that the noise contribution from the leakage current is negligible at 0°C. The depletion voltage is 60–80 V, and the total capacitance has been found to be between 2–4 pF per channel. This allows to achieve the required energy resolution of $\sim$1.5 keV. The capacitance and leakage current of the RC chip are at most 1.5 pF and 0.1 nA per channel, respectively, at the depletion voltage of $\sim$20 V, and thus the contribution to the noise is small.

3 Setup and gamma-ray response

We studied the X-ray response of DSSD and RC chips readout with the VA32TA. Here we use DSSDs with a strip pitch of 400 μm. Since n-strips intrinsically have a larger capacitance, being the Ohmic contact in this p^+-n diode geometry, we use them only for position measurements and mainly p-strips for pulse-height measurements. The p-strips were DC-coupled to the readout electronics while the n-strips were coupled through two RC chips to the VA32TA. We set the reverse bias voltage to the DSSD to 100V, and to the RC chips to 20V and 50V, respectively, as shown in figure 1. Two RC chips were used in order to reduce the voltage across the coupling capacitance and thus reduce the danger of dielectric breakdown. We biased the guard ring at the same voltage as the strips. 64 strips on each side are readout by two VA32TA chips, which is set up by the VA-DAQ provided by IDEAS, with a LabVIEW software interface. The peaking time of the shaped signal pulse is

set to 3 μs, based on the optimization study of setup parameters[10].

We measured the gamma-ray response of the DSSDs at -10 °C, by exposing them to various radio-isotopes. The pedestal of each channel was calculated by averaging the pulse-height for each data set over $\sim$ 3000 events with no hits, and we estimated the common mode noise of each event by averaging the pulse-height over the channels with no hits. The root-mean-square of the common mode noise is typically 0.5–0.6 keV (Si). The pedestal and common mode noise are subtracted from the ADC channel. The linearity function is obtained from the six gamma-ray lines of 13.927, 17.506, 20.895, and 59.54 keV from ^{241}Am and 14.4 and 122.06 keV from ^{57}Co. The response of the system in the full energy range is not linear, with a residual of $\pm$0.6 keV, due to the amplifier characteristics. Such a large residual leads to incorrect reconstruction of the Compton scattering and affects the angular resolution. We introduce an empirical formula $E = a - b\exp(-\mathrm{CH}/c)$, where E is a gamma-ray energy in keV, CH is an ADC channel, and a, b, c are free parameters, to reduce the residual to < 0.1 keV. We confirmed that the gain is stable, by measuring the variation of the photo-peak channel. The pulse-height ratio of n-strips to p-strips for the same gamma-ray energy is 0.57 for one DSSD and 0.48 for another. This is due to the charge loss caused by the capacitance of DSSDs and RC chips, which cannot be neglected in comparison with the coupling capacitance.

Figure 2 shows the pulse-height spectrum of ^{57}Co, obtained for all p-strips on one DSSD. The photopeaks of 14, 122, and 135 keV are clearly seen in the spectrum, and the broad line structure around $\sim$ 85 keV is due to the back scattering by surrounding materials. We also see a clear separation of the Pb Kα_1 and Kα_2 (74.97 and 72.80 keV) from the ambient Pb shield. The energy resolution (FWHM) of one DSSD is 1.13 ± 0.02 keV and 1.32 ± 0.03 keV for the peak of 14 keV and 122 keV, respectively, and the noise estimated as a root-mean-square of the pulse height for strips with signal below threshold is 1.02 ± 0.01 keV. The expected noise of the VA32TA is $(0.37 + 0.16 \times C_d)/\sqrt{\tau}$ (FWHM, keV) where C_d is the load capacitance in pF and τ is the shaping time in μs, which gives 0.77 keV for $C_d = 6.0$ pF and $\tau = 3$ μs. The shot and thermal noise were estimated to be 0.38 keV and 0.36 keV respectively, by assuming that the leakage current decreases by a factor of two as the temperature decreases by 7 degree. Then the total expected noise is 0.93 keV, and 1.03 keV when including the poisson noise for the 122 keV gamma-ray. The experimental values are somewhat worse than the predicted ones, possibly due to the contribution of unidentified noise sources.

Figure 3 shows the two-dimensional distribution of detected gamma-rays (122 keV) in the DSSD, together with the one-dimensional count distribution for p and n strips. Here we chose events for which the signal is within 4σ around 122 keV. Although more photons are detected around the central region due to the

inhomogeneous illumination with gamma-rays, the count distribution in each strip almost follows a Poisson distribution. Since the mean free path of 122 keV gamma-ray is longer than the DSSD thickness, the flatness of the count distribution indicates that the signal charge is efficiently collected everywhere.

We have also investigated the ratio of split events, in which the signal charge is shared between two strips. An event is defined as a split event when the neighboring p-strips give a signal above the threshold as well as a single n-strip or two neighboring n-strips. We selected events for which the sum of their p-strip signals is within 4σ of the photo-peak line. The number ratio of split events to total events is $7.6 \pm 0.2\%$, $3.4 \pm 0.1\%$, and $0.026 \pm 0.003\%$ for 122, 59.5, and 17.6 keV, respectively. Since the range of photo-electrons is longer for higher energy gamma-rays, the ratio of split events increases with energy. We also confirmed that the number ratio of split events is almost constant for all strips. We consider that the ratio of split events is not significant for soft gamma-ray detection.

4 Compton imaging

Combining the two DSSD systems, we performed the Compton imaging to measure the angular resolution[14]. We configured the Compton camera by placing the two DSSDs in parallel with a gap of 6.7 mm. The ^{57}Co gamma-ray source was placed 56.4 mm away from the DSSDs, and collimated by a 2 mm diameter hole through a 2mm thick Pb sheet. The experiment was performed at -10 °C. In figure 4, we show the scatter-plot of E_1 and E_2, which are the energy deposits of two hit channels in the Compton camera and ordered as $E_1 < E_2$. We can see the two diagonal lines corresponding to the Compton-scattering and split events for 122 keV and 136 keV gamma-ray lines emitted from the ^{57}Co source.

We selected Compton scattering events as follows. We first choose events with an energy deposition > 10 keV in at least two p-strips ($E_2 > E_1 > 10$ keV). Based on the Compton kinematics for 122 keV gamma-rays, we exclude events with $E_1 > 45$ keV. Furthermore, in the case that the two p-strips are adjacent, we consider it as a split event and discard it. We also discard the events whose signal at the n-strip on the same detector is different from that of the p-strips by more than 8 keV. We accepted events for which the total energy $E = E_1 + E_2$ is within the energy resolution of $2\sigma \sim 1.3$ keV from 122 keV. 33% of all Compton-scattering events occurred in two DSSDs, and 70% of those events are forward scattering events. The total energy distribution is Gaussian with a FWHM of 1.8 keV, which is reasonable when considering that E_1 and E_2 have a FWHM of 1.3 keV.

After selecting the Compton events, we reconstructed the incident direction of gamma-rays (figure 5). The order of hits in the Compton scattering of 122 keV gamma-ray is explicitly determined; the hit with the lower energy deposition occurs first. The axis $\boldsymbol{v}$ of the Compton cone is determined by the vector pointing from the second hit position $\boldsymbol{p_2}$ to the first $\boldsymbol{p_1}$ ($\boldsymbol{v} = \boldsymbol{p_1} - \boldsymbol{p_2}$). The scattering angle $\theta_{\rm sc}$ is calculated from the energy deposited by both hits as $\cos\theta_{\rm sc} = 1 + \frac{m_e c^2}{E_1+E_2} - \frac{m_e c^2}{E_2}$. We obtained the reconstructed image of the gamma-ray source by intersecting the Compton cone around the axis $\boldsymbol{v}$ with an arbitrary plane. Here we set the plane at the same distance as the source. Figure 6(a) shows the successfully reconstructed image of the gamma-ray source. To evaluate the angular resolution, we defined the angle $\theta_{\rm geo}$ of the vector $\boldsymbol{v}$ with the vector $\boldsymbol{u} = \boldsymbol{p_0} - \boldsymbol{p_1}$, where $\boldsymbol{p_0}$ is the center of the source. The difference $\delta\theta = \theta_{\rm sc} - \theta_{\rm geo}$ should be 0 for ideal reconstruction of an ideal point source. The measured distribution of $\delta\theta$ is shown in figure 6(b), with a FWHM of ~ 8 degree.

In order to check whether the FWHM of the above angular distribution is reasonable for the setup of this experiment, we performed a simulation using the Geant 4.5.1 package. The simulation was carried out by defining the geometry of the experimental setup, injecting the gamma-ray, and reconstructing the image in the same way as for real data. The standard process in the Geant 4 does not include the effect of Doppler broadening, so we replaced the original process of the Low-Energy Compton scattering with the G4LECS ver 1.03 provided by R. M. Kippen [15]. The simulation data agreed quite well with the experiment. The FWHM value mainly reflects four effects: (a) Doppler broadening, (b) energy resolution, (c) position resolution of the DSSD, and (d) finite size of the gamma-ray source. We individually included these effects step-by-step in the simulation, to investigate how they affect the FWHM. The energy resolution was set to 1.3 keV.

When only the effect (a) (the Doppler broadening) is included in the simulation, the angular distribution $f_{DB}(\theta)$ is described by two Gaussians with a sigma of 1.30 degree and 6.18 degree. Next, we performed the simulation including all four effects, and obtained an angular distribution $f_{all}(\theta)$ which is broader than $f_{DB}(\theta)$. In order to evaluate the effects (b)+(c)+(d), we compared the distribution $f_{all}(\theta)$ with that obtained by convolving $f_{DB}(\theta)$ with the Gaussian $\exp(-\theta^2/2\sigma^2)$, and found the best-fit σ by scanning it. This value of σ represents the contribution to the broadening other than the Doppler. It is found that $f_{all}(\theta)$ can be reproduced with $\sigma = 1.67 \pm 0.65$ degree. We also compared the distribution $f_{DB}(\theta)$ with the experimental one, by convolving $f_{DB}(\theta)$ with a Gaussian and obtained $\sigma = 2.36 \pm 0.56$ degree. Therefore we concluded that the experimental FWHM is reasonable. In the multi-layer configuration of the Compton camera, most of the hits occur at larger separation, and effect (c) becomes smaller. In a first approximation, the angular resolution of a DSSD multi-layer Compton camera corresponds to the case of (a)+(b).

It can be shown that the effect (b) is at most $\sigma = 0.80 \pm 0.33$ degree by proceeding in the same way as above.

5 Conclusion

We fabricated a prototype Compton camera system with two DSSDs read out with a VA32TA frontend chip. The energy resolution for 122 keV gamma-rays was 1.3 keV (FWHM) for the DC-coupled p-strips. This resolution is good enough to approach the Doppler-broadening limit for the angular resolution of the Compton camera. We also constructed a two-layer DSSD Compton camera and confirmed that the angular resolution achieved is compatible with the prediction.

As described in this paper, the noise is dominated by the load capacitance and the frontend amplifier noise. Our goal is to construct a Compton camera using DSSDs with a larger size of 5×5 cm^2, and thus the strip capacitance becomes larger, increasing the input noise. Therefore, it is useful to reduce the input capacitance by splitting the strips into two and pay the price of doubling the number of electric channels. We also plan to further reduce the electric noise by optimizing the frontend MOS-FET and reduce the electric power of the readout chip.

References

[1] T. Kamae, R. Enomoto, and N. Hanada, "A new method to measure energy, direction, and polarization of gamma rays," *Nucl. Inst. and Meth. A* **260**, p. 254, 1987.

[2] T. Kamae, N. Hanada, and R. Enomoto, "Prototype design of multiple Compton gamma-ray camera," *IEEE Trans. Nucl. Sci.* **35**, p. 352, 1988.

[3] T. Takahashi, K. Nakazawa, T. Kamae, H. Tajima, Y. Fukazawa, M. Nomachi, and M. Kokubun, "High Resolution CdTe Detector and its Application to the Next Generation Multi Compton Telescope," in *X-ray and Gamma-ray Telescopes and Instruments for Astronomy*, *Proc. SPIE* **4851**, p. 1228, 2002.

[4] T. Takahashi, K. Makishima, Y. Fukazawa, M. Kokubun, K. Nakazawa, M. Nomachi, H. Tajima, M. Tashiro, and Y. Terada, "Hard X-ray and Gamma-Ray Detectors for the NEXT mission," *New Astronomy Reviews* **48**, p. 309, 2004.

[5] H. Tajima, T. Kamae, S. Uno, T. Nakamoto, Y. Fukazawa, T. Mitani, T. Takahashi, K. Nakazawa, Y. Okada, and M. Nomachi, "Low Noise Double-Sided Silicon Strip Detector for Multiple-Compton Gamma-ray Telescope," in

X-ray and Gamma-ray Telescopes and Instruments for Astronomy, *Proc. SPIE* **4851**, p. 875, 2002.

[6] H. Tajima, T. Nakamoto, T. Tanaka, S. Uno, T. Mitani, E. Silva, Y. Fukazawa, T. Kamae, G. Madejski, D. Marlow, K. Nakazawa, M. Nomachi, Y. Okada, and T. Takahashi, "Performance of a Low Noise Front-end ASIC for Si/Cdte Detectors in Compton Gamma-ray Telescope," *IEEE Trans. Nucl. Sci.* **in press**, 2004.

[7] T. Mitani *et al.*, "Performance of Compton Camera using High Resolution Si/CdTe detectors – Si/CdTe Compton camera as a polarimeter –," *IEEE Trans. Nucl. Sci.* **in press**, 2004.

[8] H. Tajima, "Gamma-ray polarimetry," *Nucl. Instrum. Methods A* **511**, p. 287, 2003.

[9] H. Tajima *et al.*, "Gamma-ray Polarimetry with Compton Telescope," *Proc. SPIE* **5488**, 2004.

[10] Y. Fukazawa, T. Nakamoto, N. Sawamoto, S. Uno, T. Ohsugi, H. Tajima, T. Takahashi, T. Mitani, T. Tanaka, , and K. Nakazawa, "Low-noise Double-sided Silicon Strip Detector for Soft Gamma-ray Compton Camera," *Proc. SPIE* **5501**, p. 197, 2004.

[11] T. Tanaka, T. Mitani, S. Watanabe, K. Nakazawa, K. Oonuki, G. Sato, T. Takahashi, K. Tamura, H. Nakamura, M. Nomachi, T. Nakamoto, and Y. Fukazawa, "Development of a Si/CdTe semiconductor Compton telescope," *Proc. SPIE* **5501**, p. 229, 2004.

[12] M. Yokoyama *et al.*, "Radiation hardness of VA1 with sub-micron process technology," *IEEE Trans. Nucl. Sci.* **48**, p. 440, 2001.

[13] S. Uno, "Development of low-noise double-sided silicon strip detector for cosmic gamma-rays," *Master Thesis in Japanese i(Hiroshima University)* , 2003.

[14] T. Nakamoto, "Development of multi-layer silicon strip detector and BGO/Photodiode for soft gamma-ray Compton camera," *Master Thesis in Japanese (Hiroshima University)* , 2004.

[15] R. M. Kippen, "The GEANT low energy Compton scattering (GLECS) package for use in simulating advanced Compton telescopes," *New Astronomy Reviews* **48**, p. 221, 2004.

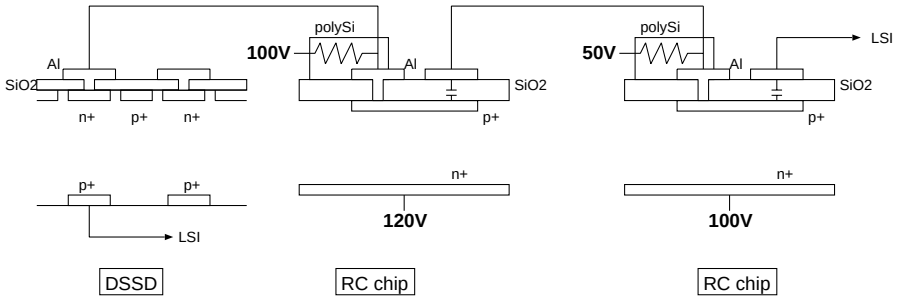

Fig. 1. Schematics of the biasing circuit of the DSSD.

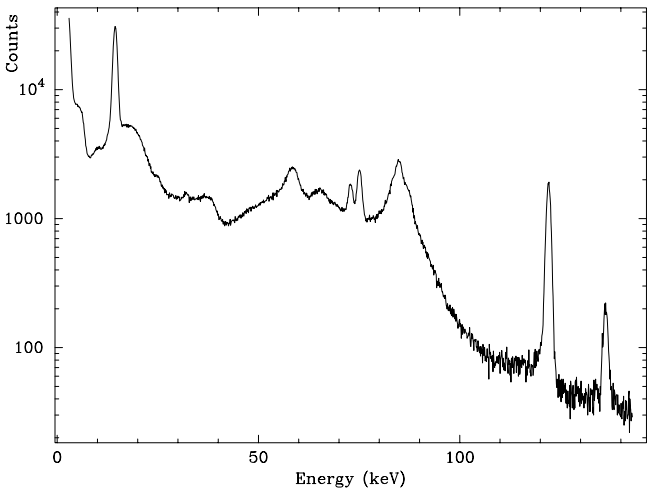

Fig. 2. Pulse height spectrum for the ^{57}Co irradiation, measured with all p-strips on one DSSD.

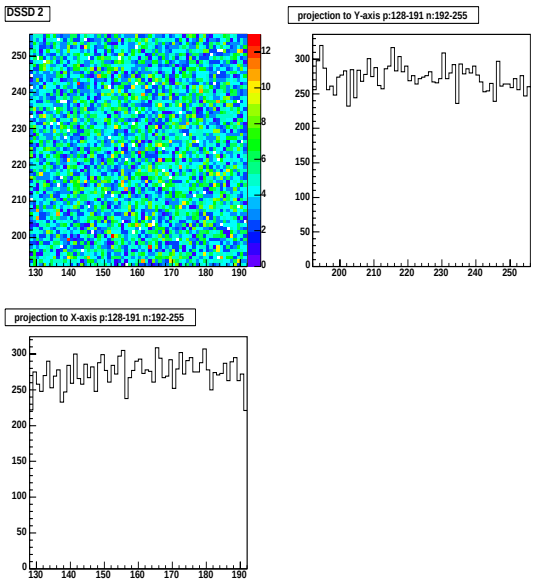

Fig. 3. The top left panel shows the two-dimensional distribution of detected 122 keV gamma-rays in the DSSD. The one-dimensional count distribution for n- and p-strips are shown at the top right and the bottom left, respectively.

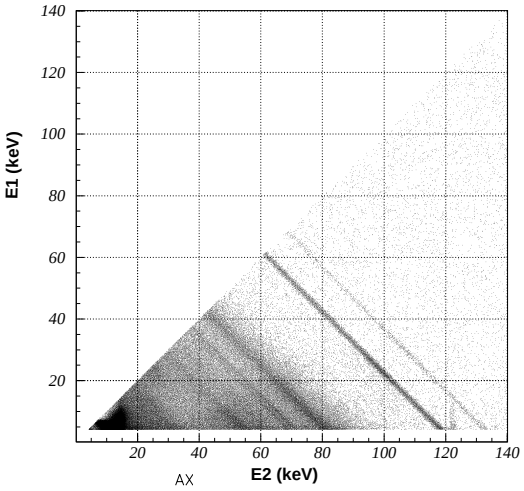

Fig. 4. The scatter-plot of E_1 and E_2. The vertical line around 122 keV is due to accidental coincidences.

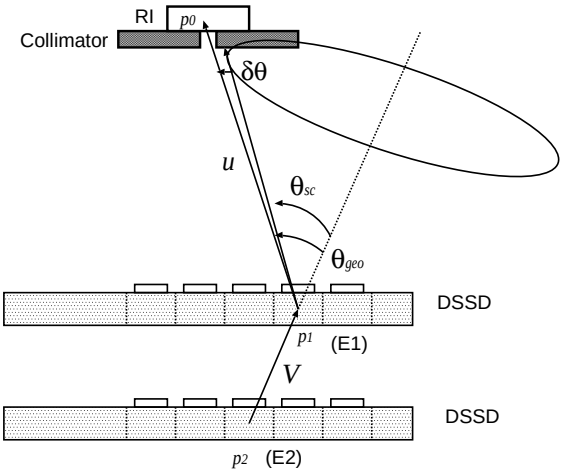

Fig. 5. Reconstruction of the direction of the incident gamma-rays.

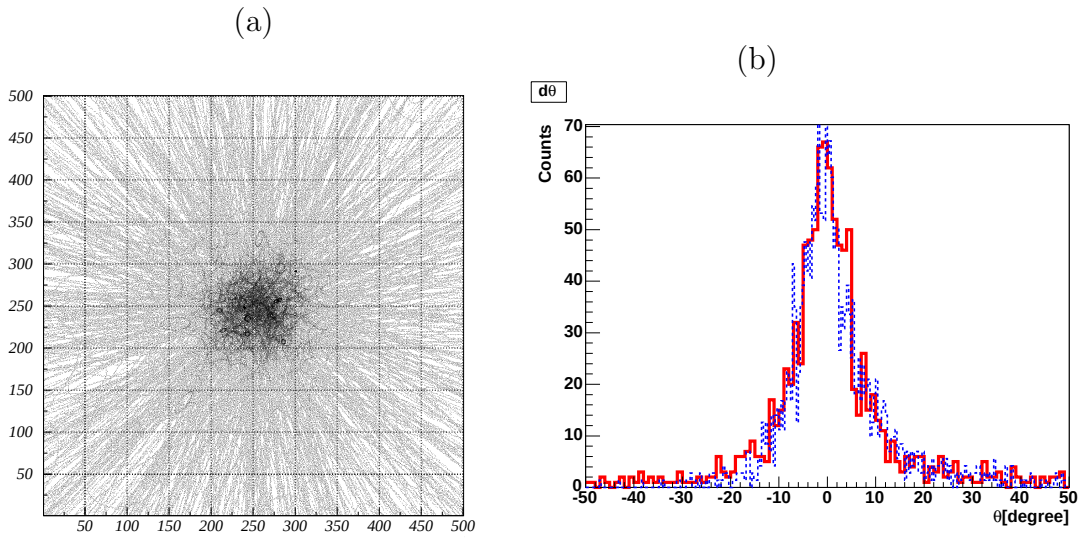

Fig. 6. (a) Reconstructed image of the 122 keV gamma-ray source. (b) Histogram of $\delta\theta$. The solid and dashed line represent the experimental data and simulation, respectively (details in the text).